J|A|C|S
ARTICLES
Published on Web 05/31/2002

Excited State Proton Transfer in Reverse Micelles

Boiko Cohen,[†] Dan Huppert,*[,†] Kyril M. Solntsev,[‡] Yossi Tsfadia,[§] Esther Nachliel,[§] and Menachem Gutman[§]

Contribution from the Raymond and Beverly Sackler Faculty of Exact Sciences, School of Chemistry, Tel Aviv University, Ramat Aviv 69978, Israel, School of Chemistry and Biochemistry, Georgia Institute of Technology, Atlanta, Georgia 30332-0400, and Laser Laboratory for Fast Reactions in Biology, Department of Biochemistry, The George S. Wise Faculty of Life Sciences, Tel Aviv University, Ramat Aviv 69978, Israel

Received December 3, 2001

Abstract: The aqueous phase of water/AOT reversed micelles having varying diameters was probed by a single free diffusing proton that was released form a hydrophilic photoacid molecule (2-naphthol-6,8-disulfonate). The fluorescence decay signals were reconstructed through the geminate recombination algorithm, accounting for the reversible nature of the proton-transfer reactions at the surface of the excited molecule and at the water/detergent interface. The radial diffusion of the proton inside the aqueous phase was calculated accounting for both the entropy of dilution and the total electrostatic energy of the ion pair, consisting of the pair-energy and self-energy of the ions. The analysis implied that micellar surface must be modeled with atomic resolution, assuming that the sulfono residue protrudes above the water/hydrocarbon interface by ~2 Å. The analysis of the fluorescence decay curves implies that the molecule is located in a solvent with physical−chemical properties very similar to bulk water, except for the dielectric constant. For reversed micelles with $r_{max} \geq 16$ Å, the dielectric constant of the aqueous phase was ~70 and for smaller micelles, where ~60% of the water molecule is in contact with the van der Waals surface of the micelle, it is as low as 60. This reduction is a reflection of the increased fraction of water molecule that is in close interaction with the micelle surface.

Introduction

Reverse micelles are nanometer-sized droplets of water, or polar solvent, that are surrounded by a layer of surfactant molecules (such as AerosolOT) and immersed in a nonpolar solvent. The polar headgroups of the surfactant molecules point inward, toward the polar solvent pool, and the alkyl chains point outward, toward the bulk organic solvent.

The general properties of reverse micelles, their interior phase, and variation of micelle size have been extensively studied.[1−17] The size of a micelle in a suspension is characterized by the molar ratio of polar solvent to surfactant:

$$w_0 = \frac{[\text{polar solvent}]}{[\text{surfactant}]} \quad (1)$$

which has been shown to be directly proportional to the micellar radius. For water/AOT reverse micelles, the radius $r_{max} = 2.3w_0$ Å. Reverse micelles tend to be spherical in shape at low surfactant and polar solvent concentrations.

These structures exhibit a high density of negative charge residues, ~65 Å^2 per SO_3^- moiety, that protrudes above the water /hydrocarbon boundary layer, forming an ordered matrix of fixed charges with counterions trapped between them. Because of the variable diameter of the reverse micelles, they are used as a model system for biological structures such as a protein surface or microcavity surrounded by phospholipids or protein matrix, with special emphasis on the complex interrelation between the fixed charges, the mobile counterions, and the solvent.

Dielectric relaxation measurements[18,19] of the electrostatic properties of reverse micelles, below their percolation limit,

* Corresponding author. E-mail: huppert@tulip.tau.ac.il.
[†] School of Chemistry, Tel Aviv University.
[‡] Georgia Institute of Technology.
[§] Department of Biochemistry, Tel Aviv University.

(1) De Gennes, P. G.; Taupin, C. *J. Phys. Chem.* **1982**, *86*, 2294.
(2) Luisi, P. L.; Straub, B. E., Eds. *Reverse Micelles*; Plenum: New York, 1984.
(3) Langevin, D. *Acc. Chem. Res.* **1988**, *21*, 255.
(4) Chevalier, Y.; Zemb, T. *Rep. Prog. Phys.* **1990**, *53*, 279.
(5) De, T. K.; Maitra, A. *Adv. Colloid Interface Sci.* **1995**, *59*, 95.
(6) Moulik, S. P.; Paul, B. K. *Adv. Colloid Interface Sci.* **1998**, *78*, 99.
(7) Gelbart, W. M.; Ben-Shaul, A.; Roux, D. *Micelles, Membranes, Microemulsions and Monolayers*; Springer-Verlag: New York, 1994.
(8) Gelbart, W. M.; Ben-Shaul, A. *J. Phys. Chem.* **1996**, *100*, 13169.
(9) Schulman, J. H.; Stoeckenius, W.; Prince, L. M. *J. Phys. Chem.* **1959**, *63*, 1677.
(10) Wong, M.; Thomas, J. K.; Grätzel, M. *J. Am. Chem. Soc.* **1976**, *98*, 2391.
(11) Zulauf, M.; Eicke, H.-F. *J. Phys. Chem.* **1979**, *83*, 480.
(12) Robinson, B. H.; Toprakcioglu, C.; Dore, J. C. *J. Chem. Soc., Faraday Trans. 1* **1984**, *80*, 13.
(13) Langevin, D. In *Structure and Reactivity in Reverse Micelles*; Pileni, M. P., Ed.; Elsevier: Amsterdam, The Netherlands, 1989.
(14) Faeder, J.; Ladanyi, B. M. *J. Phys. Chem. B* **2000**, *104*, 1033.
(15) Faeder, J.; Ladanyi, B. M. *J. Phys. Chem. B* **2001**, *105*, 11148.
(16) da Graca Miguel, M.; Burrows, H. D.; Escaroupa Pereira, M. A.; Varela, A. P. *Colloids Surf., A* **2001**, *176*, 85.
(17) Premachandran, R. S.; Banerjee, S.; Wu, K.; John, V. T.; McPherson, G. L.; Akkara, J.; Ayyagari, M.; Kaplan, D. *Macromolecules* **1996**, *29*, 6452.
(18) Kozlovich, N.; Puzenko, A.; Alexandrov, Y.; Feldman, Y. *Phys. Rev. E* **1998**, *58*, 2179.

indicated that for a reverse micelle with $w_0 = 10$ ($r_{max} = 23$ Å), the dissociated headgroups are only ~2−3% of the total population and the number of free Na^+ ions per micelle is ~1. Thus, the inner space of the micelle offered very limited ionic screening with respect to a charged molecule trapped in the micelle, despite the high "formal" concentration of counterions. Similar conclusions can be derived from the molecular dynamics (MD) calculations of Ladanyi et al.,[14] where three layers were noticed for the aqueous phase. The layer most adjacent to the hydrocarbon matrix is 2.5 Å deep and the centers of the fixed sulfono anions are well ordered and fixed on the surface. The counterions are distributed between the fixed charges forming a lattice ("the lattice layer"). In the second layer, the counterions are looser ("diffused layer"), yet their probability density is higher, and their diffusion coefficient is lower than in the rest of the micellar space that is termed "free". The precise properties and relative distribution of the counterions among the layers vary with w_0. At low w_0 values, the counterions are mostly in the lattice and the diffusion layers, but at $w_0 > 7$ the probability of finding a free ion increases to more than 10%. The characteristic of the water molecules also changes between the layers. The one closest to the hydrocarbon boundary is referred to as "trapped" and includes ~20% of the water molecules. The second layer is considered as "bound" on the basis of the number of hydrogen bonds and amounts to ~30% or less of the total water content. The free water molecules are defined as bulk and are remote by 6−7 Å from the hydrocarbon boundary. Thus, the inner space of the micelle exhibits gradients in the properties of both the counterions and the aqueous space.

Time-resolved fluorescence has been used by several groups to characterize the solvation response in reverse micelles on the femtosecond, picosecond,[20−23] and nanosecond[24−28] time scales. They found that the components of the major dynamic response occur on longer time scales than those found in bulk water or other polar solvents. Significant portions of this response are attributed to the highly restricted mobility of water, and particularly to bound and trapped water, inside the reverse micelles. In addition, even the short-time components of the solvation response appear to be longer as compared with the bulk.

Bardez et al.[29,30] and Politi et al.[31,32] have studied the excited-state proton-transfer rate in aqueous reverse micelles using several proton emitters such as 2-naphthol (2NOH) and sulfonated 2-naphthol sodium salt derivatives. It was found that the hydrophilic compound 2-naphthol-6,8-disulfonate (2N68DS), when added to water/reverse micelles with $w_0 > 8$, transferred a proton to the water at about the same rate as bulk water. In contrast to the above results, the hydrophobic 2NOH was unable to transfer a proton in a solution of reverse micelles of any size. The interpretation of Bardez is that charged photoacids, like 2-naphthol sulfonate derivatives, are placed on the ground state at about the center of the water pool of a reverse micelle in contrast to the case of 2NOH, which is dissolved in the hydrophobic surrounding.[29,30]

In the present study we shall investigate the system chemically identical with that studied by Bardez et al.[29,30] However, we are the first to demonstrate that the complexity of the system studied leads to the intricate nonexponential proton-transfer reaction kinetic. Using the geminate recombination formalism, we get new information about the water inside the micellar space, the dielectric constant of the aqueous phase, the diffusion coefficient of the hydronium ion, and the activity of the water at the formal contact surface of the proton emitter molecule. It is the custom in proton-transfer reactions to include one water shell in the reaction sphere. Thus the actual proton-transfer reaction sphere is about 6−7 Å from the center of the naphthol molecule. The measurements also monitor the water activity at the surface of the micelle. In this study we shall try to account for the reactions proceeding through the whole reaction space: at the surface of the excited molecule (where Bardez[29,30] focused her attention), at the water molecules that are in contact with the sulfono residues, and those located between the two boundaries, through which the proton should diffuse while going from the center of the micelle toward its surface. All these parameters were determined by the reconstruction of the measured signal by the geminate recombination algorithm, using the SSDP program of Krissinel and Agmon.[33] This program is based on a continuum model of the reaction space, but in the present case it was been modified to account for the following: (1) the effect of the dielectric boundary between the water and the detergent using the analytic expression introduced by Gilson and Honig[34] for calculation of the electrostatic potential inside a low dielectric matrix surrounded by water and adapted by Gutman and co-workers[35,36] for the case of a small water body engulfed by a hydrocarbon matrix, and (2) for the protrusion of the sulfono residues into the aqueous phase, as detailed in the model of Ladanyi.[14]

The combination of these models accurately reconstructed the fluorescence decay curves of the molecule, 2N68DS, and the results indicated that, when $w_0 > 5$, the intramicellar space is filled with water, the properties of which are very close to those of bulk water.

Experimental Section

Chemicals. 2-Naphthol-6,8-disulfonate (2N68DS, Kodak, >99%, chemically pure) was used without further purification. AerosolOT (AOT, Aldrich) was purified by using the procedure described in ref 37. Deionized water (resistivity > 10 MΩ/cm) was used. All other chemicals were used without further purification.

Sample Preparation. AOT was dissolved in *n*-hexane with a constant concentration of 0.1 M. After adding a known amount of water

(19) Feldman, Y.; Kozlovich, N.; Nir, I.; Garti, N.; Archipov, V.; Idiyatullin, Z.; Zuev, Y.; Fedotov, V. *J. Phys. Chem.* **1996**, *100*, 3745.
(20) Riter, R. E.; Kimmel, J. R.; Undiks, E. P.; Levinger, N. E. *J. Phys. Chem. B* **1997**, *101*, 8292.
(21) Willard, D. M.; Riter, R. E.; Levinger, N. E. *J. Am. Chem. Soc.* **1998**, *120*, 4151.
(22) Riter, R. E.; Willard, D. M.; Levinger, N. E. *J. Phys. Chem. B* **1998**, *102*, 2705.
(23) Levinger, N. E. *Curr. Opin. Colloid Interface Sci.* **2000**, *5*, 118.
(24) Sarkar, N.; Das, K.; Datta, A.; Das, S.; Bhattacharyya, K. *J. Phys. Chem.* **1996**, *100*, 10523.
(25) Mandal, D.; Datta, A.; Pal, S. K.; Bhattacharyya, K. *J. Phys. Chem. B* **1998**, *102*, 9070.
(26) Raju, B. B.; Costa, S. M. B. *Phys. Chem. Chem. Phys.* **1999**, *1*, 5029.
(27) Nandi, N.; Bagchi, B. *J. Phys. Chem. B* **1997**, *101*, 10954.
(28) Shirota, H.; Horie, K. *J. Phys. Chem. B* **1999**, *103*, 1437.
(29) Bardez, E.; Goguillon, B.-T.; Keh, E.; Valeur, B. *J. Phys. Chem.* **1984**, *88*, 1909.
(30) Bardez, E.; Monnier, E.; Valeur, B. *J. Phys. Chem.* **1985**, *89*, 5031.
(31) Politi, M. J.; Brandt, O.; Fendler, J. H. *J. Phys. Chem.* **1985**, *89*, 2345.
(32) Politi, M. J.; Chaimovich, H. *J. Phys. Chem.* **1986**, *90*, 282.
(33) Krissinel', E. B.; Agmon, N. *J. Comput. Chem.* **1996**, *17*, 1085.
(34) Gilson, M. K.; Rashin, A.; Fine, R.; Honig, B. *J. Mol. Biol.* **1985**, *183*, 503.
(35) Shimoni, E.; Tsfadia, Y.; Nachliel, E.; Gutman, M. *Biophys. J.* **1993**, *64*, 472.
(36) Bransburg, Z. S.; Fried, O.; Marantz, Y.; Nachliel, E.; Gutman, M. *Biochim. Biophys. Acta* **2000**, *1458*, 120.
(37) Rogers, J.; Winsor, P. A. *J. Colloid Interface Sci.* **1969**, *30*, 247.

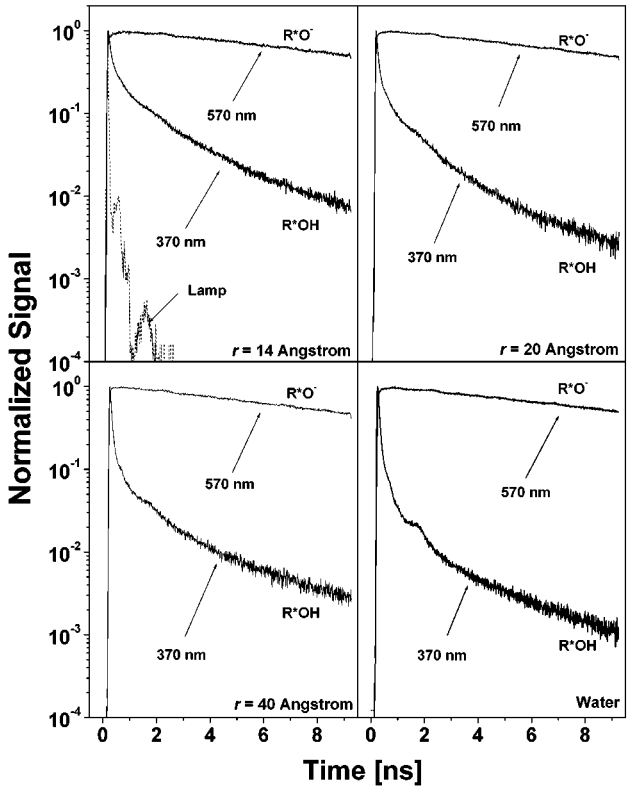

Figure 1. The R*OH and R*O$^-$ time-resolved emissions of 2N68DS in water and reverse micellar systems of $w_0 = 20$, $w_0 = 10$, and $w_0 = 7$. The upper curve, in each panel, reflects the emission measured for the anionic form of the proton emitter at 570 nm.

to the binary AOT/*n*-hexane mixture, the sample was thoroughly shaken and then sonicated for 5 min, to achieve a homogeneous ternary mixture. Dye concentrations were kept between 10^{-4} and 10^{-5} M. According to our calculation[38] less than one dye molecule per micelle was observed in the experiments.

Apparatus. Time-resolved fluorescence was measured by using the time-correlated single-photon counting (TCSPC) technique. We used a cw mode-locked Nd:YAG-pumped dye laser (Coherent Nd:YAG Antares and a 702 dye laser) providing a high repetition rate (>1 MHz) of short pulses (40 ps at full width half-maximum, fwhm) in the spectral range 285−315 nm.

The purpose of this work is to extract, from the measured fluorescence signals of the excited naphthol (R*OH) and its anion (R*O$^-$), the relevant parameters that affect the proton dynamics in reverse micelles. This is a demanding task in which one has to overcome (i) the excited state decay, (ii) low count numbers in the tails, and (iii) aberrations due to secondary peaks in the instrument response function (IRF). We partially overcome these obstacles by the standard methods of (i) accumulating relatively large counts per channel and (ii) convolution with the IRF. The counts at the peak maximum were 10 000−15 000. Figure 1 shows the raw R*OH data on the 10 ns scale, together with the IRF. It exhibits secondary parasitic peaks (less than 1% of main peak intensity) around 0.3 and 1.5 ns. These are seen to affect the measured signal for samples that decay fast to low count numbers. The secondary peaks occur in relatively physically insignificant time regions and limit mildly the accuracy of our measurement. In some of the TCSPC signals a small RF modulation at ~380 MHz can be seen. This noise does not affect the short-time component or the very long time components, but has some mild interference with the ~1 ns components.

(38) Based on the ratio [Naphthol] ≪ ([AOT]/*N*), where [Naphthol] and [AOT] are molar concentrations of 2N68DS and AOT. Values of AOT aggregation numbers *N* at different w_0 were taken from the following: Bridge, N. J.; Fletcher, P. D. I. *J. Chem. Soc., Faraday Trans. 1* **1983**, *79*, 2161.

Results and Discussion

Measurements with Lipophilic Proton Emitter. When 2NOH, an uncharged molecule, is added to the microemulsion at any w_0 value, the excited molecule exhibits no spectral evidence for dissociation in the excited state.[29,30] Apparently the preferred environment for the molecule is a poorly hydrated space, where no acceptor may react with the dissociable proton within the 9 ns lifetime of the excited state. The rest of the reported study was carried out with the hydrophilic compound 2N68DS (p$K_a = 9.0$) that, when dissolved in a microemulsion containing relatively large reverse micelles ($w_0 = 5$), has an excited-state proton-transfer rate, comparable to that measured in pure water, of about (50 ps)$^{-1}$. The dependence of the fluorescence spectra of 2N68DS on the size of the micelles was the same as observed by Bardez et al. (see Figure 4 in ref 30).

Figure 1 shows both the R*OH and R*O$^-$ time-resolved emissions of 2N68DS in water and reverse micellar systems of $w_0 = 20$, $w_0 = 10$, and $w_0 = 7$. The upper curve, in each panel, reflects the emission measured for the anionic form of the proton emitter at 570 nm. The curves exhibit a finite rise time followed by a slow decay. The rise time is attributed to the dissociation of proton from the excited molecule, while the decay reflects the radiative plus nonradiative decay of the excited molecule. The emission at 370 nm is of the R*OH molecule and is characterized by an initial fast decay that corresponds with the dissociation of the excited molecule. With time, the relaxation is slowed due to geminate recombination between the ejected proton and the excited molecule. Finally, the curvature declines in a process indicating an approach to a state of quasiequilibrium, where the velocity of dissociation and recombination are equalized. Comparison between the four panels reveals that the velocity of the fluorescence decay at 370 nm decreases in the following order: water, $w_0 = 20$, $w_0 = 10$, and $w_0 = 7$. Thus, even if the micellar radii are sufficiently large to have a well-developed "free water" population,[14] the experimental observations readily detect a clear effect of the micellar radius on the dynamics of the reaction. In the following sections we shall demonstrate how this correlation can be reproduced by incorporation of both physical and chemical considerations into the reaction mechanism.

Modeling of the Reaction Mechanism. The geminate recombination dynamics are affected by the following parameters: the rate constants of proton transfer and its recombination on the surface of the reaction sphere ($r = a$); the mutual diffusion coefficient of the proton with respect to the anion $D = D_{H^+} + D_{RO^-}$ (90% of it comes from D_{H^+}); the electrostatic potential of the proton−anion pair, and the self-energy of both ions as they vary with their location inside the micellar space. The calculation of the total potential will be described later on.

The experimental data were compared with a Smoluchowski approach for the relative diffusive motion of the geminate proton−anion pair.[39−43] According to this model, the probability density that the pair is separated by a distance r at time t after

(39) Pines, E.; Huppert, D. *J. Chem. Phys.* **1986**, *84*, 3576.
(40) Pines, E.; Huppert, D.; Agmon, N. *J. Chem. Phys.* **1988**, *88*, 5620.
(41) Agmon, N.; Pines, E.; Huppert, D. *Chem. Phys.* **1988**, *88*, 5631.
(42) Goldberg, S. Y.; Pines, E.; Huppert, D. *Chem. Phys. Lett.* **1992**, *192*, 77.
(43) Agmon, N.; Huppert, D.; Masad, A.; Pines, E. *J. Phys. Chem.* **1991**, *95*, 10407. Erratum: Agmon, N.; Huppert, D.; Masad, A.; Pines, E. *J. Phys. Chem.* **1992**, *96*, 2020.

the excitation is assumed to obey a spherically symmetric[44] diffusion equation.

$$\partial p(r,t)/\partial t = Dr^{-2}\frac{\partial}{\partial r}r^2 e^{-V(r)}\frac{\partial}{\partial r}e^{V(r)}p(r,t) - p(r,t)/\tau'_f \quad (2)$$

The mutual attraction of the proton and the 2N68DS anion, as described by a distance-dependent potential, $V(r)$ in terms of the thermal energy k_BT, was calculated by the analytic expression of Gilson and Honig[34] as adapted for a high dielectric constant body imbedded in a low dielectric matrix.[35] Fluorescence lifetime of proton−anion pair τ'_f was determined from R*O$^-$ lifetime measurements.

The gradient of the electrostatic potential affects the evolution of the reaction through modulation of the proton's probability density in the inner site of the shell, where the electrostatic potential gradient is high. In the case where the steepest gradient is close to the anion's reaction sphere, the rate of recombination will be high. In cases where the steepest gradient is close to the micellar surface, the entropic tendency to reduce the proton's probability density will drive the proton toward the micelle's outer boundary, until it is repelled by the electrostatic gradient. As a result, the most probable location for hydronium ion will be remote from the excited 2N68DS anion and hence will reduce the rate of the recombination.

The reversibility of the reaction is described by the "back reaction" boundary condition

$$4\pi a^2 D e^{-V(a)}\frac{\partial}{\partial r}e^{V(r)}p(r,t)|_{r=a} = -\kappa_d p(*,t) + \kappa_a p(a,t) \quad (3)$$

Here a is the distance of closest approach ("contact radius") between proton and anion, and the bimolecular recombination rate constant, $k_r = 4\pi a^2\kappa_a N'$, where $N' = 6 \times 10^{20}$, and $k_d = \kappa_d$ are the rate parameters for association and dissociation, respectively. In the present case we considered two reactive boundaries: one at the surface of the 2N68DS* anion, and the other at the water−AOT interface where proton reacts reversibly with the sulfono anion.

The kinetics of the bound state, the probability of which is denoted by $p(*, t)$, obey an ordinary differential equation

$$dp(*,t)/dt = \kappa_a p(a,t) - \kappa_d p(*,t) - \frac{p(*,t)}{\tau_f} \quad (4)$$

The first two terms are due to the contact reaction described by the boundary condition in eq 4, while the last term depicts the radiative decay of the excited R*OH acid. Thus, the initial condition is

$$p(*,0) = 1, \qquad p(r,0) = 0 \quad (5)$$

Subsequently, the bound and dissociated states evolve according to eqs 2 and 4, respectively. We solved these equations numerically, convoluted $p(*, t)$ with the instrument response function of the time-correlated single-photon counting system (IRF), and compared it with the measured time-resolved R*OH fluorescence.

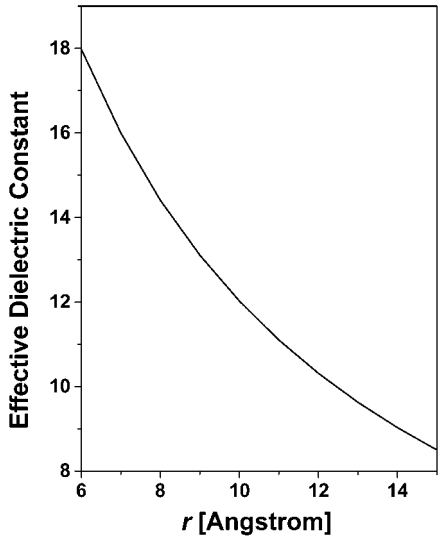

Figure 2. The variation of the calculated effective dielectric constant ϵ_{eff} as a function of the radial position of the proton for spherical reverse micelle with $r_{max} = 15$ Å. The values were calculated, given the lipid phase a dielectric constant $\epsilon_{lipid} = 8.5$ and for the aqueous phase $\epsilon_{water} = 70$.

Calculation of the Electrostatic Interactions. Gilson et al.[34] calculated the electrostatic interaction between charges in a spherical symmetric volume of low dielectric matter surrounded by water. The same formalism is applicable for the reverse situation, where a charge is confined inside a spherical water space surrounded by low dielectric matter.[35]

According to Gilson et al.,[34] the electrostatic potential of an ion pair within the water sphere consists of two components; both are a function of the relative position of the charges and their distance from the center of the water sphere. One is the Coulomb potential $G_{ij} = Q_iQ_j/\epsilon_{eff}(r)r_{ij}$ and the other is the self-energy $G_{ii} = Q_i^2/2\epsilon r_{ii}$, where Q_i and Q_j are the charges, r_{jj} and r_{ii} are the radii of the charges, and r_{ij} is the distance between the charges. ϵ_{eff} is the effective dielectric constant, which varies with the position of each charge from the center of the water sphere and with the position of the particles inside the micellar space. In practice, ϵ_{eff} is a proportional factor that relates the electrostatic attraction with the distance in order to maintain the equality $G_{ij} = Q_iQ_j/\epsilon_{eff}(r)r_{ij}$, while the G_{ij} term is calculated according to the Poisson−Boltzmann equation.

The Intramicellar Electrostatic Potential. The variation of ϵ_{eff} with the position of the proton is presented in Figure 2. The calculations were carried out in the space defined by $a \le r \le r_{max}$. Close to the surface of the excited molecule, the effective dielectric constant is high, and decreases rapidly when the proton approaches the micellar surface. While the effective dielectric constant is intuitively acceptable, it has no physical meaning and it is better to base the analysis on parameters whose values are constant, namely ϵ_{water} and ϵ_{lipid}.

The total potential of the pair, G_{tot}, is the sum of the Coulomb potential and the self-energy.[34] The equations of Gilson et al. were adapted to calculate the electrostatic interactions between proton and R*O$^-$ located at the center of a reverse micelle. For the sake of symmetry, the initial position of the proton emitter

(44) 2N68DS is not spherical symmetric with respect to the proton reaction; however, spherical symmetry assumption holds when the molecular rotation time, τ_r, is much smaller than the diffusion time of the proton from the AOT surface, τ_D, $\tau_r \ll \tau_D$ ($\tau_r \approx 70$ ps for 2N68DS in bulk water). We measured τ_r in reversed micelles so far only for HPTS (8-hydroxy-1,3,6-trisulfonate sodium salt) in its deprotonated form R*O$^-$. We found in bulk water that $\tau_r = 100$ ps, and in large reverse micelles $r > 38$ Å it is the same as in bulk water. For smaller droplets, the rotation time increases when the radius decreases. For $w_0 = 5$, $r \sim 12$ Å we find $\tau_r = 300$ ps. The diffusion time for the rebinding of the proton depends on the droplet radius. For $w_0 = 14$, the radius is $r \sim 30$ Å, the diffusion constant is $D = 3.5 \times 10^{-5}$ cm^2 s^{-1}, and the rebinding time is ~1 ns. Since we measured the proton dynamics in relatively large droplets, 12 Å < r < 90 Å, the spherical symmetry assumption is rather good.

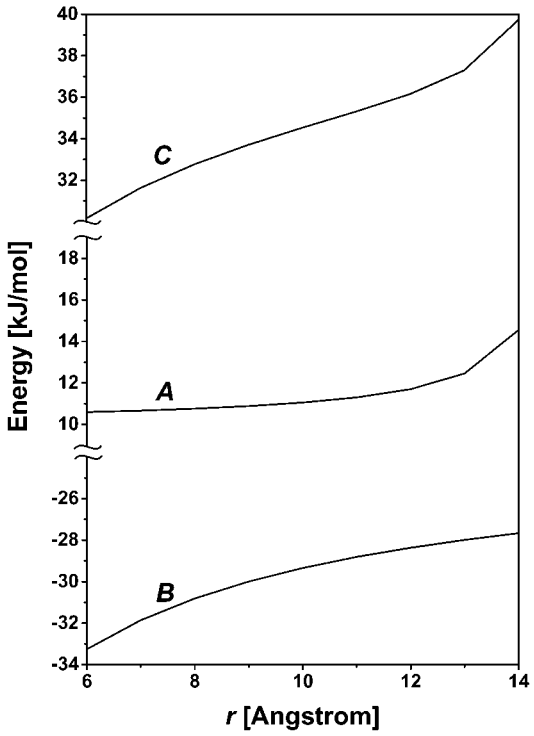

Figure 3. The variation of (A) the proton's self-energy, G_{ii}, (B) the ion-pair energy (G_{ij}), and (C) the summation, G_{tot}, as a function of the radial position of the proton as calculated for a micelle with $r_{max} = 15$ Å with $\epsilon_{water} = 70$ and $\epsilon_{lipid} = 8.5$

is in the center, as Shimoni et al.[35] indicated that an off-center position will not make a large difference in energy.

Figure 3, curves A, B, and C, depicts the variation of these parameters as a function of the radial position of the proton as calculated for a micelle with $r_{max} = 15$ Å, with $\epsilon_{water} = 70$ and $\epsilon_{lipid} = 8.5$ (for the reason for selecting these values, see below). Curve A in Figure 3 depicts the spatial variation of the proton's self-energy. The self-energy is positive over the whole space but it varies with the location. As long as the proton is within 12 Å from the micellar center, its self-energy is practically constant, but when the proton approaches the last 2 Å from r_{max}, there is a marked increase of the self-energy and only within the last 2 Å does it rise steeply, and for this reason the plot of curve A in Figure 3 extends to 14 Å. The self-energy of the anion, which is regarded as fixed in space, is positive and constant (not shown).

The ion-pair energy (G_{ij}) is presented by curve B, Figure 3. The pair energy is negative in value and its variation with r_{ij} has the shape of an asymptotic curve. The amplitude is a function of the dielectric constants of the water and the surrounding medium (not shown).

The summation, G_{tot}, of the three parameters (G_{ii}, G_{ij}, and G_{jj}) determines the total energy of the ion pair. This term is the most crucial one as it controls the propagation of the hydronium ion released from the excited 2N68DS molecule as expressed by eq 6,

$$TP_{ij} = (D_{H+}/\Delta r^2)(r_i/r_j)\exp[-\{G_{tot}(j) - G_{tot}(i)\}/2] \quad (6)$$

where TP_{ij} is the transition probability of proton transfer between two adjacent shells having a width of Δr.

The variation of G_{tot} with the relative position of the proton is presented by curve C, Figuire 3. Close to the origin, the G_{tot} function exhibits a steep increase, reflecting the contribution of G_{ij}. Toward the outer boundary of the micellar center, the G_{tot} function increases again due to the increments of the proton's self-energy. This complex behavior will, naturally, affect the transition probability of the proton and the temporal evolution of the fluorescence signal. For this reason, the effects of the dielectric constants of the water and lipid surface on the magnitude and shape of G_{tot} were investigated separately.

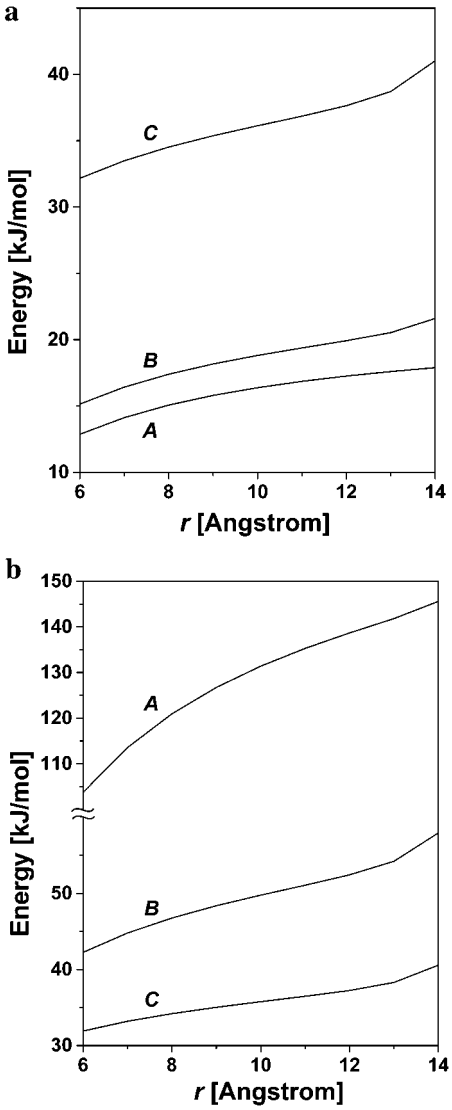

Figure 4. (a) A set of energy calculations where G_{tot} varies with r_{ij} at a constant $\epsilon_{water} = 80$ but the dielectric constant of the lipid boundary varied: 80 (curve A), 40 (curve B), and 8.5 (curve C). (b) A set of energy calculations where G_{tot} varies with r_{ij} at a constant $\epsilon_{lipid} = 8.5$ but the dielectric constant at the center of the water core varied: 10 (curve A), 40 (curve B), and 80 (curve C).

Figure 4a presents a set of energy calculations where G_{tot} varies with r_{ij} at a constant $\epsilon_{water} = 80$, but the dielectric constant of the lipid boundary varies in the range $8.5 \leq \epsilon \leq 80$. Two features are emphasized by the set of panels. The first one is that the $G_{tot}(0)$ value is a function of $\epsilon_{lipid.}$ Even a small variation of ϵ_{lipid} from 2 to 8.5 is sufficient to lower $G_{tot}(0)$ from 102 kJ/mol to 32 kJ/mol. Still, as the transition probability is a function of the gradient of the G_{tot} function, the fluorescence decay curve will vary with the other effect of ϵ_{lipid}, i.e. the change in the shape of the function. Curve A in Figure 4a depicts the G_{tot} function when calculated for the ion pair in water. The

curve is identical with a Coulombic potential, where the steepest section of the curve is next to the central ion. With decreasing values of ϵ_{lipid} (curves B and C, FIgure 4a) the asymptotic shape of the curve is lost and a steeper section appears next to the surface of the micelle. Figure 4b depicts the complimentary nature of the system. In this frame the dielectric constant of the micellar surface was set to be constant, while the dielectric constant of the aqueous phase was varied. At low values of ϵ_{water} the steep section of the function is close to the central anion (curve A, Figure 4b) but with higher values of ϵ_{water}, the function changes its shape and a reflecting potential appears near the micellar surface. As the reconstruction of the measured dynamics is very sensitive to the magnitude of the proton transfer, the analysis of the signals, gathered with micelles having different w_0 values (see Figure 1), can discriminate between the contribution of ϵ_{water} and ϵ_{lipid} to the temporal evolution of the fluorescence signal; the ϵ_{water} can vary with the radius of the micelle, while that of ϵ_{lipid} will be constant at all w_0 values.

The Reactivity of the Sulfono Headgroups. The dipole moment of reversed micelle microemulsions was determined by dielectric measurements of Feldman and co-workers[18] to be ~400 D. This value is consistent with only one or two free Na^+ ions per micelle, which, under the influence of an external field, move across the diameter of the micelle (~40 Å). These measurements relate macroscopic dielectric properties of the system and cannot measure, on a microscopic scale, the individual components such as the molecular properties of the water or the dielectric boundary.

According to the measurements of Feldman[18] and the calculations of Ladanyi,[14] most of the sulfono residues at the interface are neutralized by Na^+ counterions. The high density of the anions and counterions at the interface, together with the nonvanishing diffusivity of the counterions that emerged from the MD calculations, imply that the interface is constructed of semifixed ion pairs and that its dielectric constant will be higher than 2. Accordingly, we adopted the value of $\epsilon_{lipid} = 8.5$ for our calculation.[18]

The average state of ionization of the surface residues does not mean that the surface is chemically inert to reaction with proton. An approaching proton can replace a sodium ion and a covalent bond RSO_3-H will be temporarily formed. The sulfono residue is a mildly strong acid with $pK_a \sim 2$, and the average dwell time of a covalent proton in the form of RSO_3H will be on the order of ~7−10 ns, a time frame short enough to allow for re-dissociation of the proton before the excited anion relaxes to the ground state. Consequently, the reconstruction of the measured fluorescence decay curves necessitates accounting for this reaction by including the protrusion of the sulfono residues above the surface of the hydrocarbon water interface.[14] The dimension of the sulfono moiety is ~6 Å in diameter. Thus, a proton approaching the micellar surface will come in contact with the proton binding sites before penetrating the space where the steep slope of G_{tot} reduces its accessibility to the sulfono-rich space. Accordingly, in the reconstruction of the experimental signals, we assumed that the proton would interact in a reversible reaction with the sulfono residues at the ($r_{max} \sim 2$ Å location, where the $Na^+_{lattice}$ probability is the highest.[14]

Reconstruction of the Fluorescence Decay Dynamics. The fitting of experimental curves by the SSDP program is attained

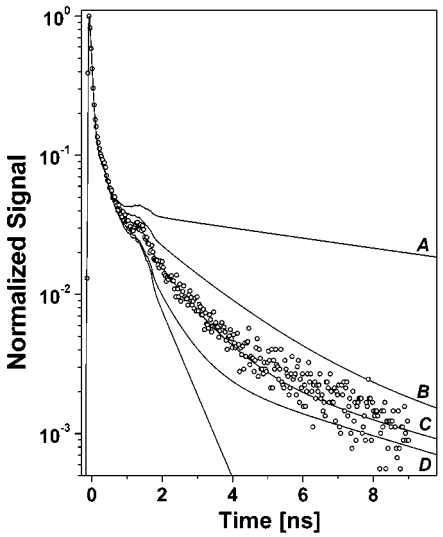

Figure 5. Reconstructed fluorescence curves that were calculated under four different boundary conditions for the reverse micelle system with $w_0 = 17$. Curve A: the outer surface of the micelle was totally reflecting. Curve B: reactive outer surface of the micelle at r_{max}. Curve C: reactive outer surface of the micelle at $r_{max} = -2$ Å. Curve D: the outer surface of the micelle was totally absorbing. Unlabeled curve: As curve D but background excluded.

by a search made over the parameter space of the following variables: (1) the rate constants of proton transfer from the excited molecule to the water and the reverse reaction (κ_d and κ_r, respectively) where the two processes take place only at the surface of the reaction sphere $r = a$; (2) the mutual diffusion coefficient of the proton (D_{H^+}) and of the R^*O^- (D_{RO^-}); and (3) the gradient of the electrostatic potential along the radius vector [in the present case the gradient was calculated for each size of micelle (calculated by the w_0 value) over a range of ϵ_{water} values and $\epsilon_{lipid} = 8.5$].

Besides these parameters, which are common to all the systems we analyzed until now, we also included a reversible reaction at the $r = (r_{max} - 2)$ Å boundary, where the proton interacts with the sulfono residues. The introduction of the reactive boundary at the terminus of the radius vector had a major effect on the shape of the reconstructed curve. For clarity, we present in Figure 5 reconstructed curves that were calculated under four different conditions. All of the curves fit the initial phase of the fluorescence decay signal, overlapping some 95% of the amplitude of the recombination process, yet the remaining 5% are more difficult to reconstruct as this is the region where the reactions at the water−micelle interface modulate the evolution of the relaxation. All curves were calculated with the same parameters that control the initial phase, but differ in the characteristics of the reactions at the boundary. Curve A in Figure 5 was calculated with parameters that fitted the initial phase of the signal while the outer surface of the micelle was totally reflective. As a result, the ejected proton was "bounced" back and the system reached a state of quasiequilibrium, where the fluorescence decay of (2N68DS···H)* did not reflect any chemical process at the outer boundary.

Curve B in Figure 5 was calculated by means of a model in which the sulfono residues were allowed to react with the proton but these proton binding sites were placed on the surface or r_{max}, i.e. at the end of the steep rise of the energy caused by the contribution of G_{H^+} to G_{tot} over the last 2 Å along the radius

Table 1. Relative Parameters for the Proton Transfer of 2N68DS in Reverse Micelles and Water

w_0[a]	r_{max}[b] [Å]	κ_d[c] [ns^{-1}]	$a_{(water)}$	κ_a [Å/ns]	k_r[d] [M^{-1} ns^{-1}]	D[e] [cm^{2}s^{-1}]	κ'_a[f] [Å/ns]	κ'_d[g] [ns^{-1}]	pK_a[h]	ϵ_i[i]
5	11.5	7.5	0.83	8.6	2.1	2.5×10^{-5}	2.8	0.045	1.5	60
7	16	10.5	0.87	12.6	3.1	2.5×10^{-5}	6	0.045	2.1	62
10	23	15.5	0.93	7.6	1.9	3.5×10^{-5}	30	0.045	2.3	72
14	32	17.5	0.96	6.1	1.5	3.5×10^{-5}	75	0.015	3.2	72
17	39	17.5	0.96	6.1	1.5	6.0×10^{-5}	65	0.025	2.9	72
20	46	18.0	0.96	7.1	1.8	7.0×10^{-5}	34	0.045	2.8	72
40	92	20.0	0.99	8.6	2.1	9.5×10^{-5}	34	0.045	2.5	74
H_2O	∞	21.0	1.00	16.5	4.1	10×10^{-5}				78

[a] Molar ratio of polar solvent to surfactant, w_0 = [polar solvent]/[surfactant]. [b] Radius of AOT/water reverse micelle. [c] Proton-transfer rate constant of 2N68DS, $k_d = \kappa_d$. [d] Proton recombination rate constant 2N68DS, $k_r \equiv 4\pi a^2 \kappa_a N'$. [e] Mutual diffusion coefficient derived by fitting the Smoluchowski model to the experimental data. [f] Proton recombination rate constant at the micelle interface. [g] Proton-transfer rate constant at the micelle interface. [h] Equilibrium constant of the proton reaction at the interface. [i] The dielectric constant at the center of the reverse micelle.

vector. In this case, the reflection of the proton back to the inner space of the micelle is milder, and some of the protons are removed by the reversible protonation of the sulfono residues. Curve C in Figure 5 was calculated according to the same conditions as curve B, except that the sulfono residues were modeled to protrude by 2 Å from the surface of the hydrocarbon matrix, as suggested by Ladanyi.[14] As a result, the protonation of the sulfono residues was only mildly affected by the partial exclusion of proton from the end of the radius vector and a good fit to the experimental curves was achievable for all measurements carried out with $w_0 > 7$. The last curve in Figure 5, D, was calculated under the assumption that any proton that reached the sulfono headgroups reacted with them irreversibly, and was removed from the system. Apparently, this model leads to a faster than measured relaxation, indicating that the dissociation of proton from the sulfono headgroups affects the process.

Panels a and b in Figure 6 consist of a set of kinetic reconstructions of signals gathered at varying w_0 values. For the best fit, the surface reactivity is modeled by a fast proton recombination with $\kappa'_a = 20$ Å/ns and a slow release of proton with $\kappa'_d = 0.05$ ns^{-1}. It should be stressed that the uncertainty of determination of these rates is rather large (±50%), and should be taken as a guideline for the surface reactivity. On the basis of these values for characterizing the reaction at the micellar surface, signals gathered with reversed micelles with varying w_0 values were analyzed. Table 1 gives the fitting parameters of the time-resolved fluorescence data. The fits are based on the G_{tot} calculation by using $\epsilon_{water} = 72$ and $\epsilon_{lipid} = 8.5$ (calculation with $7 \leq \epsilon \leq 10$ essentially yielded the same results) and by reducing the effective radius by 2 Å ($r = r_{max} - 2$) to account for the protrusion of the sulfono moiety above the water−hydrocarbon interface. Figure 6 shows the experimental data and the computer fit of the time-resolved fluorescence of the R*OH species in reverse micelles using the relevant parameters. It is of interest to point out that kinetic measurements carried out with reversed micelles having $w_0 < 5$ could not be reconstructed. Apparently, when the radius of the aqueous phase is smaller than 4 solvation shells (~12 Å), the inclusion of the 2N68DS molecule with its three sites of interaction with the water molecule stresses the micellar structure, causing deformation/swelling of the 2N68DS-containing reversed micelles to a size exceeding the one determined for "empty" reversed micelles. For these reasons, the size of the fluorophore-containing micelles deviates from the relationship given by eq 1 (see below). Because of the uncertainties concerning the size and shape of the small reversed micelles, we analyzed those with $w_0 \geq 5$, and the parameters are given in Table 1.

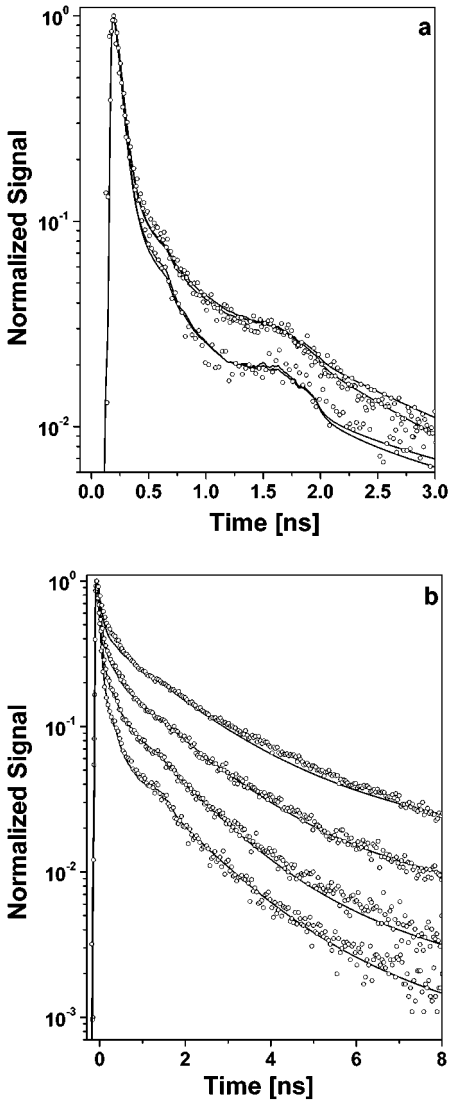

Figure 6. The experimental data (circles) and the computer fit (solid line) of the time-resolved fluorescence of the R*OH species in reverse micelles with use of the relevant parameters. (a) Bottom to top: neat water, $w_0 = 40$, $w_0 = 20$,and $w_0 = 17$. (b) Bottom to top: $w_0 = 15$, $w_0 = 10$, $w_0 = 7$, and $w_0 = 5$;

The rate constant of proton transfer, k_d, decreases as the size of the water sphere reduces. For bulk water we find $k_d = 2.1 \times 10^{10}$ s^{-1}.[45] In medium size water spheres, $30 < r_{max} < 46$ Å,

(45) Solntsev, K. M.; Huppert, D.; Agmon, N. *J. Phys. Chem. A* **2001**, *105*, 5868.

its value is 1.8×10^{10} s^{-1}. For smaller spheres, $r_{max} < 30$ Å, it continuously decreases with the radius decrease. At the smallest size studied, $r_{max} = 14$ Å, $k_d = 1.45 \times 10^{10}$ s^{-1}. The relatively small dependence of k_d on the size of the water sphere indicates that the water in all these spheres is a good proton acceptor. Using the empirical correlation between the magnitude of k_d on the water activity, $a_{(water)}$,[46] the apparent activity of the water inside the micellar space was calculated to change between 0.99 ($w_0 = 40$) and 0.81 at $w_0 = 5$. These values are comparable to the activity of the water in large aqueous spaces such as the PhoE ion-conducting channel.[36,47]

The rate of recombination, κ_a, and the second-order reaction derived from k_r (see Table 1) are in the order of $k = 6 \times 10^9$ M^{-1} s^{-1} in bulk water and are reduced to half when the compound is trapped inside the reversed micelles.

The other protonation reaction that influences the shape of the R*OH fluorescence decay is at the surface of the micelle. Two rate constants were determined, each as an independent adjustable parameter, yet the resulting ratio between the rate constants is in good agreement with the pK_a value of a sulfono residue. At the low water content, $w_0 = 7$, where the intensity of the counterions interaction with the fixed sulfono residues is increased, we observe a reduced rate of protonation of the sulfono moiety, probably due to enhanced ordering of the Na^+ ions in the "lattice" layer and stronger interaction of the Na^+ ion with the sulfono residue in the "diffuse" layer.[14]

The properties of the water in the reversed micelles, some 1000 molecules trapped in a micelle with $w_0 = 10$, can be evaluated by three parameters: (1) the activity, as deduced from κ_d, (2) the diffusion coefficient of the proton, and (3) the dielectric constant of the aqueous phase. The activity of the water in the reversed micelles was calculated from the rate of the proton transfer, yielding an index for the tendency of the water molecules, which are within the solution shell of the excited molecule, to form a solvation cluster for the proton.[46] Yet, as the solvated proton is a structure made of 4 to 5 water molecules ($H_3O^+_{aq}$ or $H_5O_2^+{}_{aq}$), its size can be some 6−9 Å, spanning most of the distance between the 2N68DS molecule and the trapped water layer. Thus, the high activity of the water represents a large fraction of the micellar space. The diffusion coefficient of the proton, determined as an independent adjustable parameter, decreased gradually with the shrinking of the micellar radius. This is in accord with the MD calculation of Ladanyi,[14] who noticed higher ordering of the water molecule and a reduced self-diffusion coefficient of the water in small radius micelles. The last parameter characterizing the water is the dielectric constant. In the present study we assumed that all of the aqueous phase inside the reversed micelles has a uniform dielectric constant and that the intensity of the electrostatic potential is determined by the dielectric boundary and the distance of the ions from the dielectric boundary. The calculation yielded a rather high dielectric constant value, which was practically constant and equal to that of bulk water. Only below $w_0 = 5$ did we notice a significant decrease of ϵ, which was coupled with a marked decrease in the proton's diffusion coefficient and lowering of the water activity. Apparently at $w_0 = 5$, the inner space of the reversed micelles is already small enough to affect the physical−chemical properties of the enclosed water.

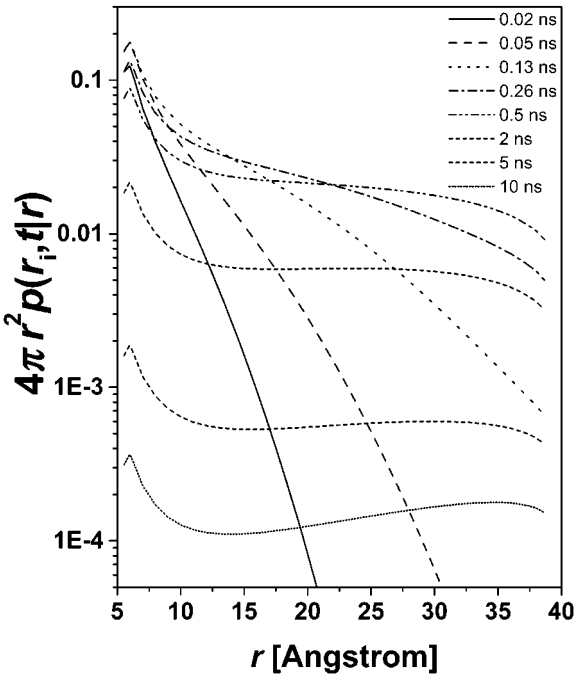

Figure 7. The temporal evolution of the radial probability distribution of the proton in the water sphere, obtained as a numerical solution of eq 2.

The Spatio-Temporal Distribution of a Proton Inside Reversed Micelles. The profile of electrostatic potential inside the reversed micelles differs from that in bulk water by having two steep domains: the proximal one is near the 2N68DS* anion, as in bulk water, while the distal one is located next to the water−hydrocarbon interface, where the image charges of the proton contribute to G_{tot}. The propagation of the proton, once released from the excited 2N68DS molecule, is controlled by the transition probabilities defined in eq 6, whose magnitude is a function of the electrostatic potential and an entropic term appearing as the ratio r_i/r_j. Very close to the 2N68DS molecule, where the radii are small, the entropic drive is very strong and the dispersion of the proton's probability density is the driving force of the dissociation process. Near the water−hydrocarbon dielectric boundary reaction, where r is already large, the entropic drive is weaker and cannot compensate for the steeper electrostatic potential. As a result, over the last few angstoms, a gradual reflective force is built and prevents the proton from approaching the dielectric boundary.

Figure 7 shows the temporal evolution of the radial probability distribution of the proton in the water sphere, obtained as a numerical solution of eq 2. At $t = 0$ the proton is bound to 2N68DS*. The excited molecule rapidly dissociated with a time constant of $\tau \sim 43$ ps, and the proton is released to the innermost concentric shell of the reaction sphere ($a = 5.5$ Å). From the reaction sphere, the proton's probability density gradually disperses over the whole volume of the reversed micelles. On a short time scale of a few tens of picoseconds, the proton distribution is almost exponential. Due to the relatively slow diffusion process, the protons are initially located near the contact distance. At longer times, $\sim 0.5-1.0$ ns, diffusion sets in, and the distribution function spreads over the whole space of the micelle. At longer times ($t > 1.4$ ns), the radial probability density attains a state of quasiequilibrium with a time-stable

(46) Gutman, M.; Nachliel, E. *Biochim. Biophys. Acta* **1990**, *1015*, 391.
(47) Gutman, M.; Tsfadia, Y.; Masad, A.; Nachliel, E. *Biochim. Biophys Acta* **1992**, *1109*, 141.

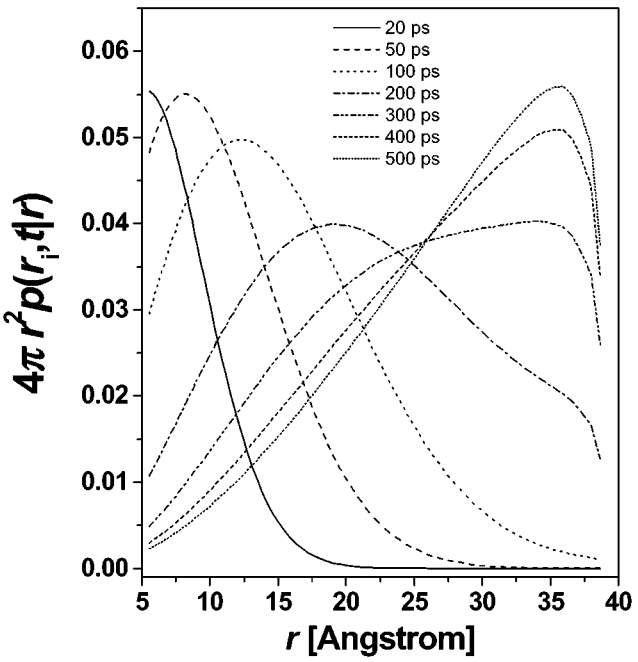

Figure 8. The temporal evolution of the probability density of a single charged particle released at the center of a reversed micelle.

minimum at ~10 Å. In parallel with the dispersion within the micellar space, the proton probability density is reduced by its reaction with the excited anion and the sulfono residues. For this reason, the *Y*-axis of Figure 7 is constantly adjusted to account for the depletion of the probability density function. The sharp decrease of the probability density, close to the center, demonstrates that the entropic driven dispersion overcomes the steep electrostatic potential gradient (see Figure 3). As the probability density function spreads, it approaches the outer boundary where the electrostatic potential exhibits a second steep phase, but the entropic drive is much smaller. As a result, the probability density forms a second maximum.

The dynamics presented in Figure 7 demonstrate how the kinetic treatment of a mobile particle can simulate an equilibrium (or quasiequilibrium) system. Thus, by setting the rate constants of the reactions at the surface of the reaction spheres (inner one at $r = a$ and outer one at $r = r_{max} - 2$), the equilibrium distribution of ions in reversed micelles can be calculated.

In the present study we incorporated into the calculation the contribution of two terms that are sometimes neglected: the entropy, which favors the reduction of the probability density of the particle by driving it toward the edge of the reversed micelle, and the self-energy that repels the charged particle from the immediate vicinity of the dielectric constant boundary. Figure 8 emphasizes the role of the two terms in reduction of the probability density of a single charged particle released at the center of a reversed micelle. The calculations were carried out by integration of the transition probabilities, calculated according to eq 2, except that the potential term is given exclusively by the ion's self-energy (the entropic term, r_i/r_j was maintained as in all other calculations). The ion was released near the center of the aqueous phase and the probability density was calculated as a function of time. In the absence of electrostatic attraction to a central counterion the dispersion is much faster (compared to the evolution of the probability density in Figure 7). At 500 ps after the laser excitation, the probability density is spread, with a maximum close to the surface, where the repulsion near the dielectric boundary balances the drive toward the outermost shell of the spherical space. It is of interest to note that this calculation of the ions distribution function in a reversed micelle is compatible with the general features deduced by Ladanyi by means of extensive MD calculation.[14]

Summary

The excited-state proton transfer and geminate proton recombination processes of 2-naphthol-6,8-disulfonate (2N68DS) sodium salt were studied in aqueous/AOT reverse micelles. We analyzed the data by the reversible diffusion-influenced reaction model with spherical symmetry. We used electrostatic potential of an ion pair within a water sphere surrounded by an outer layer of a smaller dielectric constant. We found that the data could not be fitted well when the image charge repulsion was included. We explain this as a result of the confinement of most of the sodium ions to a very small layer next to the negatively charged sulfonate groups of the AOT surface. The data analysis suggests that 2N68DS is approximately located at the center of the water pool and not at the trapped and bound water layers next to the AOT surface layer or even at the a polar exterior media. The proton-transfer rate in large-diameter water spheres ($d > 80$ Å) is about the same as that in bulk water. In intermediate spheres $80 < d < 45$ Å the rate is slightly reduced and the spherical model can be used to fit the data. At small size spheres of $d < 30$ Å, the proton-transfer rate decreases as a function of the sphere radius and the deviation of the calculated fit to the experimental data is larger.

Acknowledgment. D.H. acknowledges support by grants from the U.S.−Israel Binational Science Foundation and the James-Franck German−Israel Program in Laser-Matter Interaction. The research in the Laser Laboratory for Fast reactions in Biology is supported by the research grants from the Israeli Science Foundation 427/01-1 and the German Israeli Foundation for Research and Development (I-594-140.09/98).

JA012646C